Ni/Hβ-Zeolite Catalysts Prepared by Deposition−Precipitation

Rubén Nares,[†,‡] Jorge Ramírez,*[,†] Aída Gutiérrez-Alejandre,[†] Catherine Louis,[§] and Tatiana Klimova[†]

Departamento de Ingeniería Química, Facultad de Química, UNAM, Cd. Universitaria, México D.F., (04510), Laboratoire de Réactivité de Surface, URA1106 CNRS, Université P. et M. Curie, Place Jussieu, 75252 Paris Cedex 05, France, and Instituto Mexicano del Petróleo, Eje Central Lázaro Cárdenas, 152, 152, México, D. F., (07730)

Received: March 21, 2002; In Final Form: August 6, 2002

The deposition−precipitation (DP) method, which was extensively developed for the preparation of Ni/SiO_2, is applied here to the preparation of Ni/Hβ zeolite catalysts. The Ni/Hβ samples prepared at different deposition−precipitation times (1−4 h) were characterized by BET, XRD, TPR, FTIR, SEM, and TEM. The results indicate that as in the case of the deposition−precipitation of Ni on silica of low surface area, for short DP times (=2 h), nickel hydroxide is the main Ni(II) phase deposited on Hβ zeolite whereas, for longer DP times (3 and 4 h), the Ni(II) phase is a mixture of nickel hydroxide and 1:1 nickel phyllosilicate. The behavior of the OH groups of the Hβ zeolite indicates that the Ni(II) phase species are formed mainly on the external surface of the zeolite. After reduction at 450 °C, the samples contain well-dispersed Ni metal particles with sizes between 9.5 and 120 Å and with average particle sizes between 29 and 44 Å, depending on the DP time.

1. Introduction

The preparation of supported catalysts with high dispersion and high metal loading is a field of great interest in catalysis. Among the most used preparation methods, ion exchange can provide high metal dispersions but limited metal loadings, whereas impregnation can achieve high metal loading but a limited dispersion. To overcome the problem of the preparation of supported catalysts with high dispersion and high metal loading, several novel preparation strategies were proposed for different metal/support systems.[1−13] In the case of Ni/SiO_2 catalysts, such features can be achieved with the deposition−precipitation (DP) method developed by Geus[14−16] and then extensively studied by Burattin et al.[17−20] This method is based on the precipitation of a nickel(II) phase onto silica thanks to the slow and homogeneous basification of the solution containing the metal precursor and the support by urea hydrolysis at 90 °C. The nature of the Ni(II) phase depends on the DP time and the silica surface area.[17] For DP times shorter than 4 h, the Ni(II) phase supported on a silica of low surface area (≈50 $m^2 \cdot g^{-1}$) is a nickel hydroxide with a turbostratic structure α-Ni-$(OH)_2$ (layered compound with a disordered stacking of brucitic layers of octahedral Ni(II)), with increasing amounts of 1:1 nickel phyllosilicate at high DP times. On silica of high surface area (≈400 $m^2 \cdot g^{-1}$), 1:1 nickel phyllosilicate is the main Ni(II) phase (layered compound of structural formula $Si_2Ni_3O_5(OH)_4$, consisting of a brucite-type sheet containing Ni(II) in octahedral coordination and a sheet containing linked tetrahedral SiO_4 units). It may be noted that the source of Si for the formation of 1:1 nickel phyllosilicate is the support itself, which is gradually consumed during DP. The Ni loading increases with the DP time and ≈20 wt % of Ni are deposited after 4 h of DP. After reduction in hydrogen, highly dispersed Ni particles whose average size also depends on the DP time and on the silica surface, are obtained (from 27 to 79 Å).[18] In addition, the metal particles do not easily sinter because of their strong interaction with the support.[2,4−12,17,18] Hence, it appears interesting to attempt to apply this method to the preparation of Ni catalysts supported on zeolites with high Si/Al ratios.

Among zeolites, the β zeolite (Hβ) presents interesting properties as a support because of its three-dimensional 12-ring pore system with an intersecting channel system[21] and its rather large pores (7.6 × 6.4 Å and 5.5 × 5.5 Å).[22] This three-dimensional large pore zeolite has already found successful applications in several reactions of industrial interest.[23−31] Hence, in this study, we hope to succeed in combining the interesting properties of the β zeolite with the advantages of the deposition−precipitation method and to obtain Ni/Hβ-zeolite catalysts with high Ni loading and a homogeneous distribution of small Ni particles. In this study, special attention will be paid to the following key points: (i) determining how the structural properties of the zeolite are affected by the deposition of nickel, (ii) determining which Ni(II) phase is formed in the Hβ zeolite, and (iii) determining the location of the Ni(II) phase in the zeolite (inside the pores or/and on the external surface).

2. Experimental Section

2.1. Sample Preparation. The Hβ-zeolite sample was provided by Zeolyst International CP811E-75 (lot 1822-74; $SiO_2/Al_2O_3 = 75$, surface area =580 $m^2 \cdot g^{-1}$). The Ni/Hβ zeolite samples were prepared according to the following procedure: First, 250 mL of an aqueous solution of nickel nitrate (0.14 M) was prepared. This solution was divided in two parts: 40 mL were used to dissolve urea at room temperature and the other 210 mL were used to make a suspension with 1.9 g of Hβ zeolite (pH ≈ 2). Afterward, the zeolite suspension was heated to 70 °C and mixed with the urea dissolution. The mixture was taken

* Corresponding author. E-mail: jrs@servidor.unam.mx.
† UNICAT.
‡ Instituto Mexicano del Petróleo.
§ Université P. et M. Curie.

10.1021/jp0207679 CCC: $22.00
Published on Web 11/21/2002

to 90 °C to start the deposition−precipitation of nickel onto the Hβ zeolite. After a chosen DP time (1−4 h), the suspension was cooled to 15−20 °C and filtered and the solid was washed three times with 20 mL of distilled hot water (50−60 °C). Finally, the samples were dried at 110 °C for 24 h. Hereafter, the samples will be referred as Ni/Hβx where x, which takes values from 1 to 4, refers to the DP time expressed in hours.

2.2. Sample Characterization. The BET nitrogen adsorption−desorption isotherms were performed in an ASAP 2000 instrument using N_2 at −195 °C. Prior to the adsorption the samples were evacuated at 270 °C for 3 h. The microporous area was estimated using the correlation of t-Harkins & Jura (*t*-plot method).

The XRD diffractograms were registered with a Philips 1050/25 diffractometer using Cu Kα radiation (λ = 1.5418 Å); the goniometer speed was 1° (2θ) min^{-1}.

The FTIR spectra were performed at room temperature on a Nicolet Magna IR 760 instrument (100 scans and a resolution of 4 cm^{-1}). The samples were finely ground and dispersed in KBr with a ratio of 1:100, and then they were pressed as a pellet. To study the hydroxyl region, additional experiments were performed with self-supported pressed wafers of catalyst powder prepared with 10 mg of sample. The sample wafers were analyzed in an IR cell after activation by heating under high vacuum at 550 °C during 1 h.

Temperature programmed reduction (TPR) of the dried samples was performed in a RIG-100 In Situ Research Instruments. Before TPR the samples were heated at 150 °C for 2 h under an argon stream (40 mL·min^{-1}). The TPR conditions were the following: 125 mg of sample reduced at atmospheric pressure under a stream of 5% v/v H_2 in argon (total flow rate of 25 mL·min^{-1}), using a linear temperature program from room temperature to 1000 °C, with a heating rate of 7.5 °C·min^{-1}.

The Ni content, wt % Ni = (g of Ni/(g of NiO + g of Hβ zeolite)) × 100, of the Ni/Hβ samples was determined with a JEOL JSM-5900LV microscope equipped with an analytical EDX accessory and also by titrating a previously dissolved sample with EDTA and a murexide indicator. Differences smaller than 5% in the Ni content were found between both methods.

For the TEM study of the reduced catalysts, the samples were reduced in a quartz gas flow reactor at atmospheric pressure for 5 h at 450 °C under a flow of H_2 (50 mL·min^{-1}). The Ni metallic particles were measured with a JEOL JEM 2010 high-resolution electron microscope operating at 200 kV. The histograms of metal particle sizes were established from the measurement of at least 300 particles. The average metal particle diameter was calculated according to the equation $d_{av} = \Sigma n_i d_i / \Sigma n_i$, where n_i is the number of particles of diameter d_i.

3. Results

3.1. pH Change during DP. Figure 1 shows the variation of the solution pH during the DP time. These variations are due to the hydrolysis of urea at 90 °C, i.e., to the formation of OH^- ions, and to their consumption during the deposition−precipitation of Ni on Hβ zeolite. The shape of the curve is similar to that obtained during DP of Ni on silica.[17,32,33]

From repeated experiments, it was found that the Ni loading increases with DP time in a highly reproducible fashion and that it is possible to establish fairly accurately the change in the Ni loading as a function of DP time (Figure 2).

3.2. Characterization of Ni onto Hβ Zeolite. *3.2.1. Textural Characterization.* Figure 3 shows the N_2 adsorption−desorption isotherms of the Hβ zeolite and of the various Ni/Hβ samples.

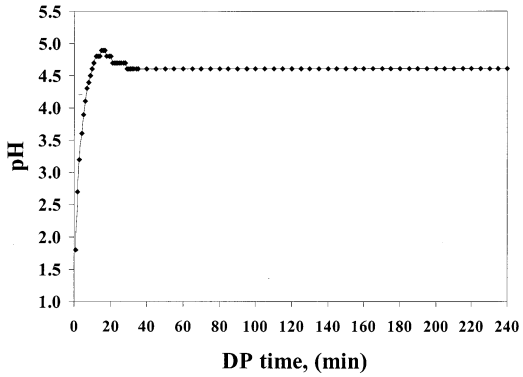

Figure 1. Evolution of the pH of the solution versus time, during deposition−precipitation of nickel on Hβ zeolite.

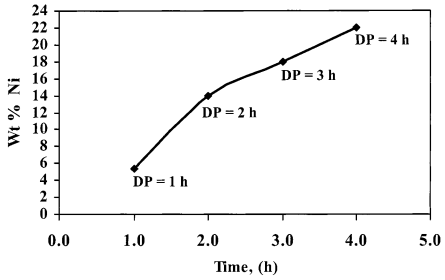

Figure 2. Changes in the Ni loading of the Ni/Hβ samples as a function of the DP time.

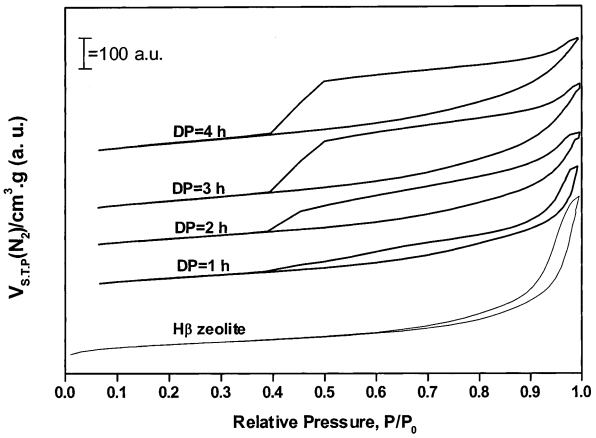

Figure 3. Nitrogen adsorption−desorption isotherms of the Hβ zeolite and Ni/Hβ samples.

Hβ zeolite shows a type I isotherm characteristic of a microporous material. The hysteresis loop at high relative pressures (P/P_o = 0.65−1.0) can be ascribed to mesoporosity between the zeolite particles. When Ni is deposited onto the zeolite, the shoulder in the desorption branch of the hysteresis loop starts at about P/P_o = 0.4. This value is intrinsic to the use of N_2 and is due to the instability of the meniscus.[34,35] This hysteresis loop exhibits the following features: (i) it extends from 0.4 to 1.0 P/P_o; (ii) it widens as the DP time increases; (iii) its shape can be assigned to B or H3 type,[34−36] characteristic of a lamellar compound. These results suggest the formation of a Ni-containing lamellar structure (possibly Ni phyllosilicate or nickel hydroxide) on the external surface of the zeolite.

Table 1 shows the variations of the total surface area, the mesoporous and the microporous surface areas, and pore volume with the DP time. The microporous surface area and pore volume of the Ni/Hβ samples decrease with the DP time. Also, the mesoporous surface area increases due to the increasing amount of Ni with the DP time, i.e., the increasing amount of

TABLE 1: Textural Properties of Hβ Zeolite and Ni/Hβ Samples Obtained at Various DP Times

	Hβ zeolite	Ni/Hβ1	Ni/Hβ2	Ni/Hβ3	Ni/Hβ4
total surface area, $m^2 \cdot g^{-1}$ [a]	580	555	520	490	452
mesoporous surface area, $m^2 \cdot g^{-1}$	221	267	320	330	332
microporous surface area, $m^2 \cdot g^{-1}$ [a]	359	288	200	160	120
microporous volume, $cm^3 \cdot g^{-1}$ [a]	0.1659	0.1331	0.094	0.072	0.053
apparent microporous surface area, $m^2 \cdot g^{-1}$		315[b]	286[b]	355[c]	333[c]
			364[c]		
estimated microporous volume, $cm^3 \cdot g^{-1}$		0.145[b]	0.118[b]	0.16[c]	0.15[c]
			0.17[c]		

[a] Per gram of Ni/Hβ. [b] Per gram of Hβ, assuming that the Ni phase is $Ni(OH)_2$. [c] Per gram of Hβ, assuming that the Ni phase is a mixture of 50% of 1:1 nickel phyllosilicate and 50% of $Ni(OH)_2$.

lamellar Ni(II) phase, nickel phyllosilicate and/or nickel hydroxide. In Table 1 we also include estimations of the microporous surface area and pore volume per gram of zeolite calculated under the assumption of different proportions of $Ni(OH)_2$ and 1:1 Ni phyllosilicate in the sample. These estimations indicate that the microporosity of the zeolite is not substantially blocked and that probably we have samples with a mixture of Ni hydroxide and 1:1 Ni phyllosilicate.

3.2.2. X-ray Diffraction. Figure 4 shows the XRD patterns of the Hβ zeolite and the Ni/Hβ samples. With respect to the Hβ zeolite sample, the XRD patterns of the Ni/Hβ samples show two new asymmetric reflections at $2\theta = 33.2$ and 59.2° with *d* spacings of 2.66 and 1.54 Å, respectively. According to a previous work,[17] these two reflections can be assigned either to the (10) and (11) reflections of turbostratic nickel hydroxide or to both the (201) and (1,3,−2,0) and the (0,6,−3,3) reflections of 1:1 nickel phyllosilicate. The intensity of these reflections increases with the DP time. This is consistent with the increasing amount of Ni deposited. However, the most characteristic reflections that permit the distinction between 1:1 nickel phyllosilicate and nickel hydroxide are the (001) reflection of both compounds between 11 and 7 Å, the (002) reflection of nickel hydroxide, and the (0,2,−1,1) and (002) reflections of 1:1 nickel phyllosilicate between 3.5 and 4.5 Å.[17] Unfortunately, the (001) and (002) reflections overlap with the reflections of the Hβ zeolite at 2 Å = 7.8 and 25.2° (with *d* spacing of 11.32 and 3.488 Å, respectively) and therefore cannot be analyzed (Figure 4). Other techniques such as TPR and IR spectroscopy will be used to attempt to discriminate between these two Ni(II) phases. Figure 4 also shows that the intensity of the main reflections of the Hβ zeolite at 2 Å = 7.8° and 22.5° (with *d* spacings of 11.32 and 3.93 Å, respectively), decrease with the DP time. This can be due to the decrease in percent zeolite in the Ni/Hβ samples as the Ni content increases and/or to a loss in the crystallinity of the sample, due to its partial dissolution during DP.

3.2.3. Temperature-Programmed Reduction. TPR of the Dried Samples. The TPR profiles of the dried Ni/Hβ samples are shown in Figure 5. At short DP time (1 h), the TPR profile shows the presence of a sharp reduction peak at 400 °C and of a smaller and broader one at about 480 °C. As the DP time increases, the sharp peak decreases and the broad one increases in intensity, shifts toward higher temperatures (480−580 °C), and splits into two peaks. Comparison of these results with those obtained previously for bulk and SiO_2-supported nickel hydroxide and nickel phyllosilicate,[5,17−19] allows us to assign the low-temperature peak (≈400 °C) to the reduction of nickel hydroxide, and the broad high-temperature peak to the reduction of 1:1 nickel phyllosilicate. However, the partial decrease of the peak at 400 °C with DP time suggests that at higher DP times the fraction of Ni forming $Ni(OH)_2$ decreases.

3.2.4. FTIR Characterization. IR Spectroscopy in the Hydroxyl Region. The IR spectrum of the Hβ zeolite in the hydroxyl region is shown in Figure 6. It shows two intense ν_{OH} bands, one asymmetric at 3745 cm^{-1}, associated with terminal SiOH groups (external OH[37,38] at 3745 cm^{-1} and internal OH[39−41] at 3740 cm^{-1}), and another one at 3610 cm^{-1}, associated with internal bridging hydroxyls,[37,38,42] responsible for the strong Brønsted acidity in zeolites. Deposition−precipitation of Ni onto the zeolite induces several effects. As the DP time increases, the band assigned to terminal silanols decreases in intensity and shifts down to 3740 cm^{-1} for sample Ni/Hβ4. This indicates a decrease in the number of external silanols of zeolite with the DP time. It is less easy to conclude whether the number of internal silanols varies. However, for short DP time (≤2 h), the band at 3610 cm^{-1} decreases significantly in intensity, suggesting the partial consumption of the internal bridged hydroxyl groups during the first stages of the deposition−precipitation process. For higher deposition times (=2 h), the formation of new hydroxyl groups associated with species other than Hβ zeolite from Ni hydrosilicates or Ni hydroxide, which appear at about 3640 cm^{-1}, is possible. These new hydroxyl groups would be responsible for the observed increase in the intensity and slight shift of the maximum of the band at 3610 cm^{-1}. Moreover, lateral interactions between the hydroxyl groups of the new Ni species and the internal bridging hydroxyl groups of the Hβ zeolite would also bring about a shift and broadening of the band.

IR Spectroscopy in the Region of Structural Vibrations. Figure 7 displays the IR spectra of the Hβ zeolite and the Ni/Hβ samples obtained by the KBr pastille method in the mid-infrared region of 2500−400 cm^{-1}. This region contains the fundamental framework vibrations of the $Si(Al)O_4$ groups.[43−45] Il-crystallized 1:1 Ni phyllosilicate also exhibits vibration bands in the 1200−400 cm^{-1} range, i.e., stretching SiO vibrations at 1005 and ≈1040 cm^{-1}, and bending vibrations of structural OH groups at 670 cm^{-1}.[8,17] Nickel hydroxide shows a band characteristic at 640 cm^{-1}.[17] All these bands overlap with those of Hβ zeolite (Figure 7), which make the assignment uneasy. However, when the DP time increases, a band at 640 cm^{-1}, characteristic of nickel hydroxide,[17] appears in the spectrum of Ni/Hβ2. At longer DP times, i.e., in the spectra of Ni/Hβ3 and Ni/Hβ4, this band increases in intensity and a shoulder becomes visible at higher wavelength (660−670 cm^{-1}). A shoulder on the low wavelength side of the band at 1085 cm^{-1} of Hβ zeolite can also be observed. It appears as a split band at 1005 and 1049 cm^{-1} on the subtraction spectrum (Figure 8). To obtain the subtraction spectrum, the Hβ zeolite was treated in the same conditions as sample Ni/Hβ4, i.e., in a urea solution at 90 °C for 4 h. The presence of bands at 670 (shoulder), 1005, and 1049 cm^{-1} indicate that samples Ni/Hβ3 and Ni/Hβ4 contain also 1:1 nickel phyllosilicate.[8,17]

In addition, the vibration bands of the Hβ zeolite at 797 cm^{-1} (symmetric stretching of SiO_4 tetrahedra[43]) and at 1085 cm^{-1}, assigned to external SiO_4[43,46] or asymmetric stretching Si−O−Al,[44] decrease with the DP time. This could be related to a dissolution process of the siliceous framework during the DP process, and in this case would support the formation of Ni hydrosilicates at the expense of the siliceous framework.

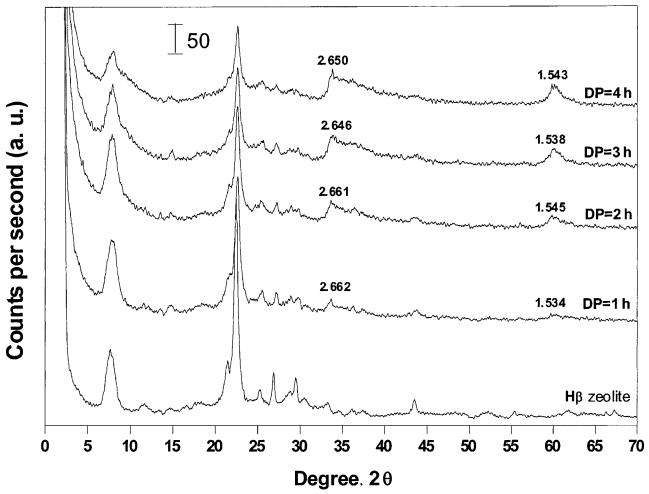

Figure 4. XRD patterns of the Hβ zeolite and Ni/Hβ samples.

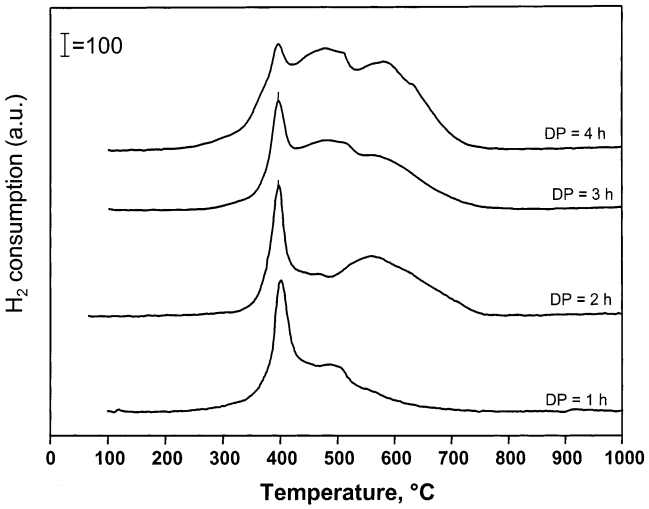

Figure 5. TPR profiles of the dried Ni/Hβ samples.

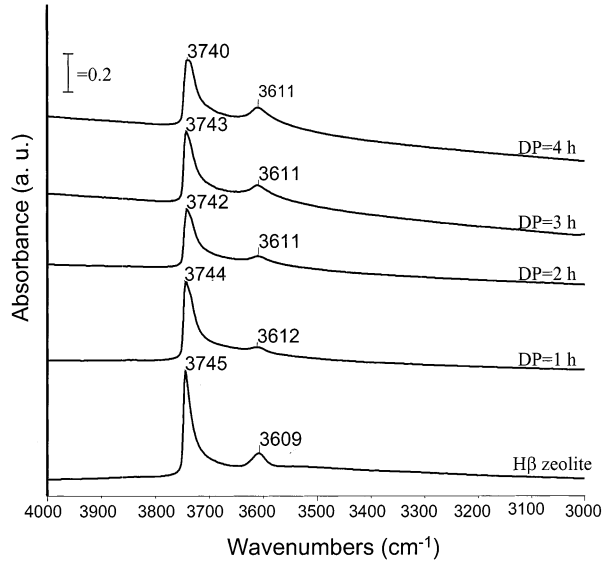

Figure 6. IR spectra of the Hβ zeolite and Ni/Hβ samples in the hydroxyl region.

During DP, a new band at 2192 cm^{-1} increases in intensity. This band has already been observed in the spectra of Ni/SiO_2 samples prepared by DP. It was attributed to isocyanate ions that arise from urea decomposition and that are located in the structure of nickel hydroxide and 1:1 nickel phyllosilicate.[17]

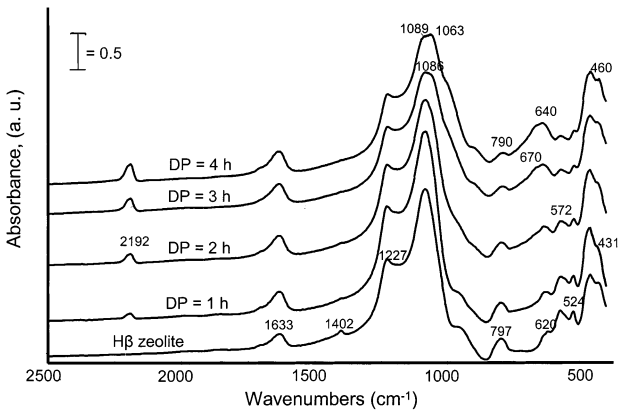

Figure 7. IR spectra of the Hβ zeolite and Ni/Hβ samples in the structural vibrations region.

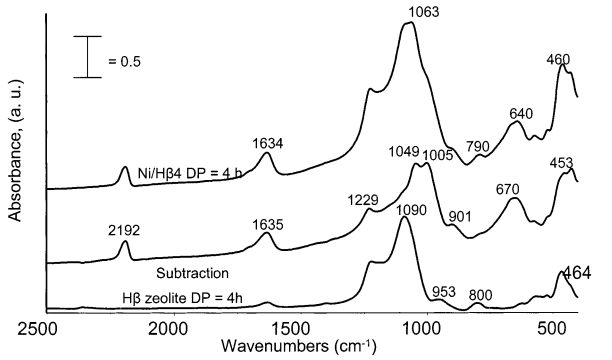

Figure 8. IR spectra of Hβ zeolite treated with urea at 90 °C during 4 h, Ni/Hβ4, and the subtraction spectrum.

3.2.5. Electron Microscopy. SEM. The SEM micrographs of the Ni/Hβ samples (Figure 9) show the appearance of a granulated surface on the zeolite particles as the DP time increases. These observations are well in line with the dissolution of part of the silica surface in the Hβ zeolite and the formation of Ni phases on the external zeolite surface.

TEM. Figure 10 displays the micrographs of samples Ni/Hβ1 and Ni/Hβ4 after drying and after reduction. In the micrographs of the dried samples, increasing formation of lamellar structures with DP time is clearly observed. The samples reduced at 450 °C for 5 h show a homogeneous distribution of Ni metallic particles. In the reduced Ni/Hβ4 sample, lamellar structures are still observed, indicating an incomplete reduction of the Ni in the silicate structures. These observations are consistent with those in Ni/SiO_2 systems.[47]

The histograms of size distribution of Ni metallic particles in the reduced Ni/Hβ samples are shown in Figure 11. The average particle size (included in Figure 11) increases with the DP time from 29 to 44 Å. Only in Ni/Hβ1 were particles smaller than 10 Å observed.

4. Discussion

The variation of the solution pH versus the DP time (Figure 1) is similar to that obtained during DP of Ni on silica.[17,32,33] In addition, the evolution of the Ni loading versus the DP time (Figure 2) is the same as for DP Ni/SiO_2, i.e., $\approx$20 wt % of Ni is deposited after 4 h of DP. One can deduce from these results that the same mechanism of deposition of nickel is involved on Hβ zeolite as on silica. As explained in the Introduction, urea hydrolysis slowly generates OH^- ions in solution, which induce first a fast increase in the solution pH. Then, as the DP time increases, pH reaches a maximum and stabilizes at a

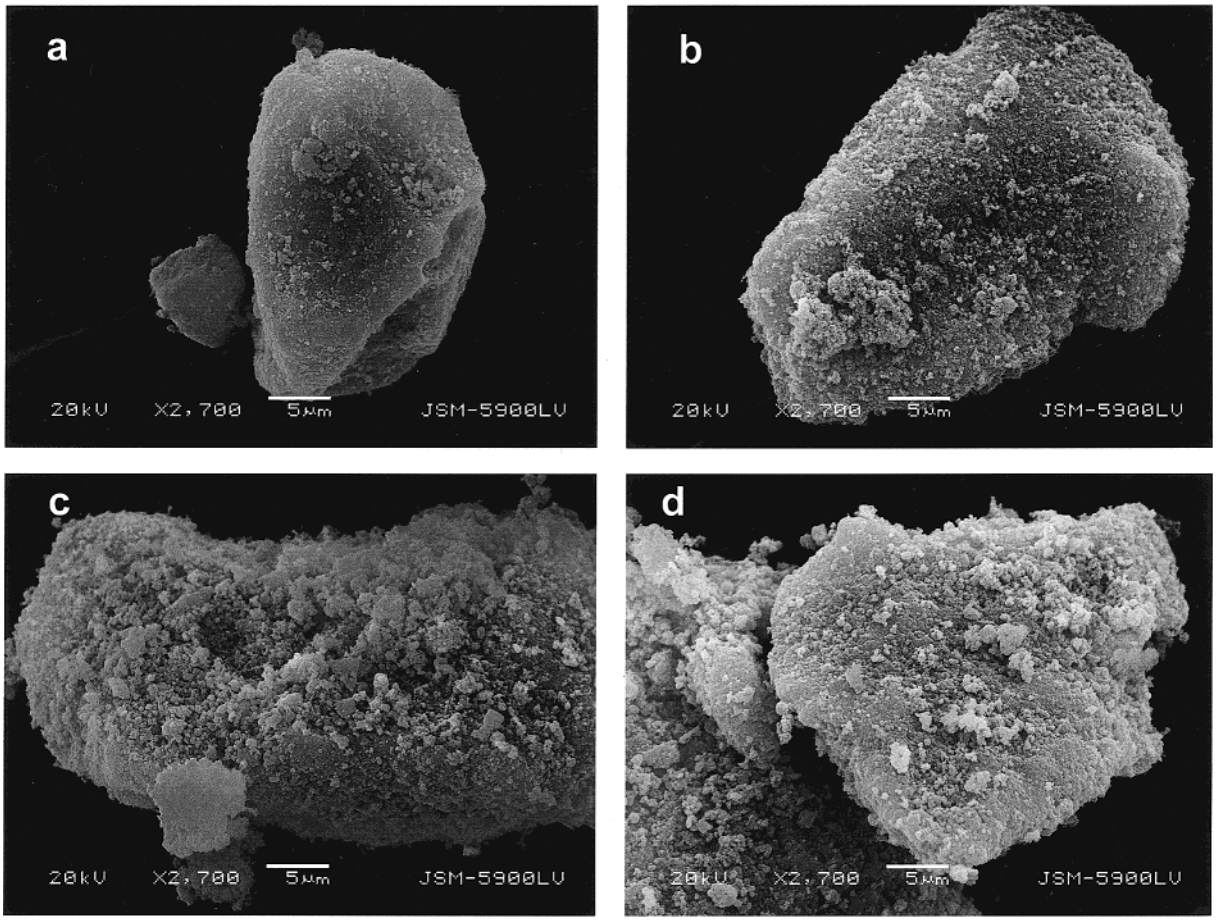

Figure 9. SEM micrographs of the dried samples: (a) Hβ zeolite; (b) Ni/Hβ1; (c) Ni/Hβ2; (d) Ni/Hβ4.

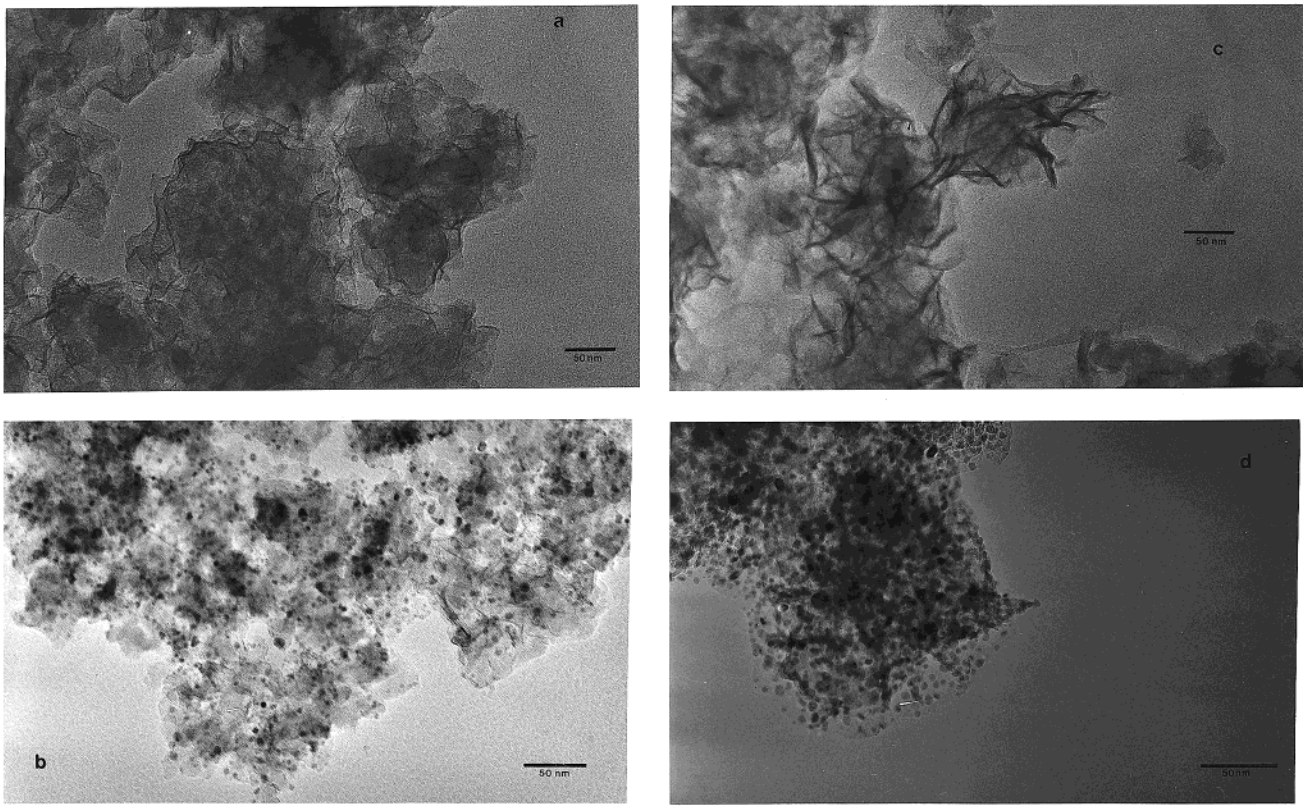

Figure 10. HREM micrographs of (a) dried Ni/Hβ1, (b) reduced Ni/Hβ1, (c) dried Ni/Hβ4, and (d) reduced Ni/Hβ4.

slightly lower value because of the establishment of a dynamic equilibrium between the formation of OH^- ions in solution and their consumption for the deposition−precipitation of the Ni(II) phase.[18] The mechanism of deposition−precipitation of Ni onto

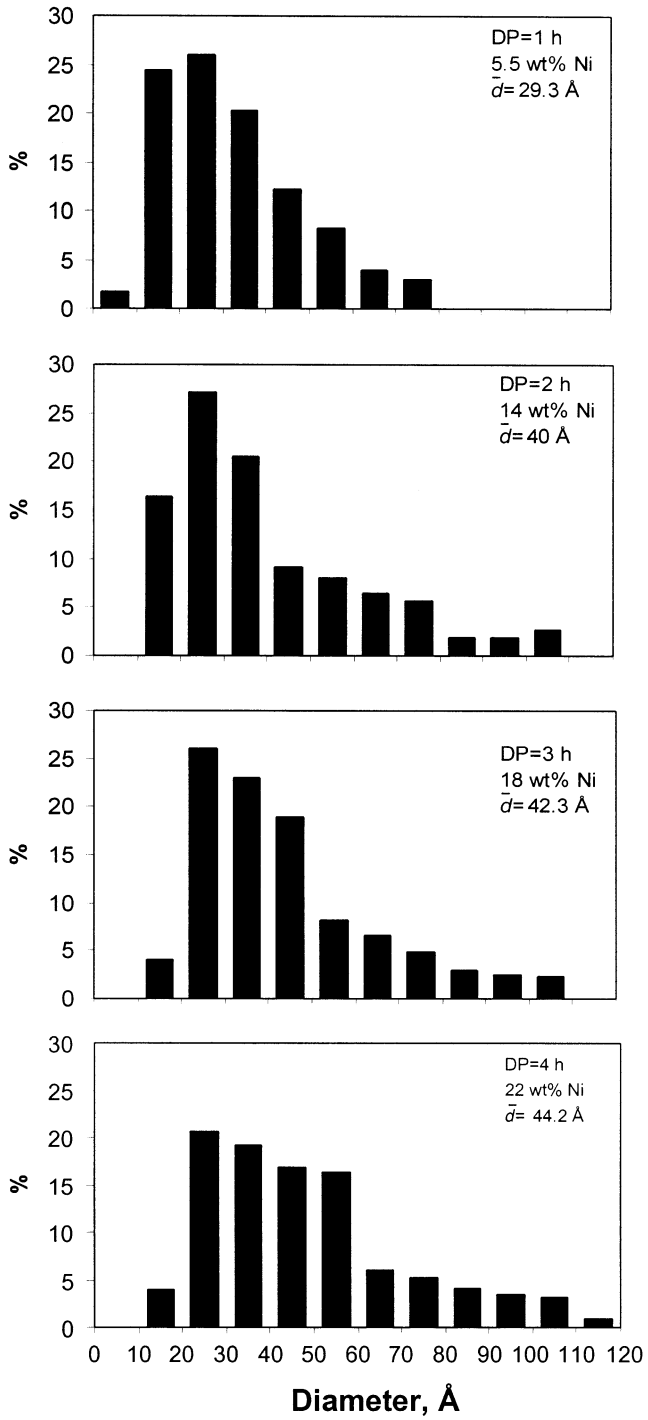

Figure 11. Size distribution histograms of Ni metal particles in Ni/Hβ samples. Values of average particle size, $\bar{d}$, are included.

SiO_2 has been explained in ref 18. It is mainly based on the kinetic competition between two types of reactions:

1. Ni−OH−Ni olation/polymerization:

$$2Ni(OH_2)_4(OH)_2 \rightarrow (HO)_2(H_2O)_3Ni{-}OH{-}Ni(OH_2)_4(OH) + H_2O$$

which leads to the formation and growth of the nickel hydroxide phase on the silica surface;

2. Ni−O−Si heterocondensation/polymerization: In this case, the dissolution of the support releases silicic acid into the solution. This silicic acid reacts with the hydrolyzed nickel complexes containing H_2O ligands through a reaction of heterocondensation of the oxolation-type, which leads to the formation of Si−O−Ni bridges:

$$Si(OH)_4 + Ni(OH_2)_4(OH)_2 \rightarrow (HO)_3Si{-}O{-}Ni(OH_2)_4(OH) + H_2O$$

and then, after polymerization, to the formation and growth of 1:1 Ni phyllosilicate onto the silica surface.

The second reaction is faster than the first one, but it is limited by the concentration and diffusion in solution of the silicic acid arising from silica dissolution.

The widening of the hysteresis loop of the N_2 adsorption−desorption isotherms of the Ni/Hβ samples with the DP time (Figure 3), and the increase in the mesoporous surface area (Table 1), are consistent with the increasing amount of Ni deposited and with the formation of a new lamellar Ni(II) phase. The granulated surface that appeared on the zeolite particles (SEM micrographs in Figure 10) as the DP time increases is also consistent with the formation of a new lamellar Ni(II) phase. This lamellar phase may be nickel phyllosilicate or nickel hydroxide or a mixture of them because both are lamellar compounds. The XRD patterns (Figure 4) did not allow us to discriminate between these two Ni(II) phases, but TPR and IR spectroscopy provided us valuable information. The evolution of the TPR peaks with the DP time (Figure 5) indicates that at the beginning of the DP, nickel hydroxide is the main species present on the Hβ zeolite. As the DP time increases, more and more 1:1 Ni phyllosilicate is formed and its crystallinity increases (leading to a splitting in the high-temperature peak). The evolution of the IR spectra versus the DP time (Figure 7) leads to the same conclusions: a band at 640 cm^{-1} characteristic of nickel hydroxide[17] appears in the Ni/Hβ2 spectrum, and three additional vibration bands at 670, 1005, and 1049 cm^{-1} characteristic of 1:1 nickel phyllosilicate[8,17] are visible in the Ni/Hβ3 and Ni/Hβ4 spectra. Hence, the Ni/Hβ samples contain mainly nickel hydroxide for DP times lower than 2 h. A growing proportion of 1:1 nickel phyllosilicate exists for 3 and 4 h of DP time.

The evolution of the TPR peaks and of the IR spectra versus the DP time look more like the changes observed during DP of Ni on a silica of low surface area (50 $m^2 \cdot g^{-1}$) than on a silica of high surface area (400 $m^2 \cdot g^{-1}$).[17] One can wonder whether this is because of the presence of the small amount of Al in the Hβ zeolite (SiO_2/Al_2O_3 molar ratio = 75), which delays the dissolution of the silicic species, or it is because the deposition of Ni occurs to a greater extent on the external surface of the Hβ zeolite.

To answer this question, it is necessary to examine the structural changes of the zeolite support itself that occur during DP:

·A decrease occurs in the intensity of the main XRD reflections of the Hβ zeolite ($2\theta = 7.8$ and 22.5° with d spacings of 11.32 and 3.93 Å, respectively), Figure 4, and of the vibration bands of the Hβ zeolite at 797 cm^{-1} (symmetric stretching of SiO_4 tetrahedra[43]) and asymmetric stretch at 1085 cm^{-1}, attributed to external SiO_4[43,46] or asymmetric stretching Si−O−Al[44] (Figure 7). All these changes are consistent with a loss in the crystallinity/structure of the Hβ zeolite, due to its dissolution/consumption for the formation of 1:1 nickel phyllosilicate.

·A decrease occurs in the number of external silanols (Figure 6); this OH consumption may indicate that the deposited Ni(II) phase interacts with them. A decrease occurs in the microporous surface area and in the pore volume of the Ni/Hβ samples (Table

1); it may be also due to the consumption of the zeolite when nickel phyllosilicate forms or/and to some blocking of the cavities or channels of the Hβ zeolite when Ni is deposited. This second hypothesis is more difficult to verify because it is not clear whether the internal silanols are involved in the OH consumption (Figure 6).

To conclude about the reason for the similarity between the evolution of the TPR profiles and IR spectra of DP of Ni on Hβ and that of DP of Ni on a silica of low surface area, we rather believe that, despite the high surface area of the zeolite, the deposition of Ni occurs mostly on the external surface of the Hβ zeolite.

After reduction of the Ni/Hβ samples, the TEM micrographs show that the average size of the Ni metallic particles (Figures 10 and 11) is small (between 29 and 44 Å) for Ni loadings from 5.5 to 22 wt %. These results are consistent with those obtained on Ni/SiO_2 samples prepared by DP and reduced at similar conditions.[46] The strong interaction between the Ni(II) phase and the Hβ zeolite notably inhibits the sintering of the nickel particles during reduction treatments and leads to small metallic particles, as in the case of Ni/SiO_2 samples prepared by deposition−precipitation.[47] It may be noted that most of the metallic particles are larger than the pore size of the Hβ zeolite, confirming that the Ni(II) phase and most of the Ni metallic particles after reduction are deposited on the external surface of the Hβ zeolite.

5. Conclusions

The following conclusions can be drawn. The deposition−precipitation of nickel on Hβ zeolite occurs in the same way as for the DP of nickel on silica of low surface area. The Ni loading increases with the DP time (1−4 h) in a highly reproducible fashion, from 5.5 to 22 wt %. For short DP times (=2 h), nickel hydroxide is the main Ni(II) phase on Hβ zeolite whereas for longer DP times (3 and 4 h), the Ni(II) phase is a mixture of nickel hydroxide and 1:1 nickel phyllosilicate. The characterization study of the Hβ support indicates that it is mostly the external surface that is involved for supporting the Ni(II) phase. It also confirms the consumption of the zeolite framework for the formation of 1:1 nickel phyllosilicate. Nickel hydroxide and 1:1 nickel phyllosilicate, which are both lamellar structures, lead to an increase in the mesoporous surface area of the samples.

Hence, the method of deposition−precipitation of nickel applied to the Hβ zeolite leads to high Ni loading and high Ni dispersion (average metallic particle size from 29 to 44 Å). However, the metallic nickel particles are mainly located on the external surface on the zeolite.

Acknowledgment. We acknowledge the financial support from the IMP FIES program. R.N. is grateful to IMP for the scholarship received. We also acknowledge Leticia Baños for the XRD work, Ivan Puente-Lee for the TEM and SEM analysis, and Rogelio Cuevas and Perla Castillo for helpful discussions.

References and Notes

(1) Houalla, M.; Delannay, F.; Matsuura, I.; Delmon, B. *J. Chem. Soc., Faraday Trans. 1* **1980**, *76*, 2128.
(2) Turlier, P.; Praliaud, H.; Moral, P.; Martin, G. A.; Dalmon, J. A. *Appl. Catal.* **1985**, *19*, 287.
(3) Mile, B.; Stirling, D.; Zammit, M. A.; Lovell, A.; Webb, M. *J. Catal*. **1988**, *114*, 217.
(4) Bonneviot, L.; Clause, O.; Che, M.; Manceau, A.; Dexpert, H. *Catal. Today* **1989**, *6*, 39.
(5) Clause, O.; Bonneviot, L.; Che, M.; Dexpert, H. *J. Catal.* **1991**. *130*, 21.
(6) Clause, O.; Kermarec, M.; Bonneviot, L.; Villain, F.; Che, M. *J. Am. Chem. Soc.* **1992**, *114*, 4709.
(7) Louis, C.; Cheng, Z. X.; Che, M. *J. Phys. Chem.* **1993**, *97*, 5703.
(8) Kermarec, M.; Carriat. J. Y.; Burattin, P.; Che, M.; Decarreau, A. *J. Phys. Chem. B* **1994**, *98*, 120.
(9) Okamoto, Y.; Nagata, K.; Adachi, T.; Inamura, K.; Takyu, T. *J. Phys. Chem. B* **1991**, *95*, 310.
(10) Carriat, J. Y.; Che, M.; Kermarec, M. *Catal. Lett.* **1994**, *25*, 127.
(11) Toupance, T.; Kermarec, M.; Louis, C. *J. Phys. Chem. B* **2000**, *104*, 965.
(12) Huong, L. L. Ph.D. Thesis, Paris, 1989.
(13) van Stiphout, P. Ph.D. Thesis, Utrecht University, 1987.
(14) Geus, J. W. Dutch Patent Applications, 1967, 6705, 259, and 1968, 6813, 236.
(15) van Dillen, J. A.; Geus, J. W.; Hermans, L. A.; van der Meijden, J. In *Proceedings of the 6th International Congress on Catalysis, London, 1976*; Bond, G. C., Wells, P. B., Tompkins, F. C., Eds.; Elsevier: Amsterdam, 1977; p 677.
(16) Verhaak, M. J. F. M.; van Dillen, A. J.; Geus, J. W. *Appl. Catal.* **1993**, *105*, 251.
(17) Burattin, P.; Che, M.; Louis, C. *J. Phys. Chem. B* **1997**, *101*, 7060.
(18) Burattin, P.; Che, M.; Louis, C. *J. Phys. Chem. B* **1998**, *102*, 2722.
(19) Burattin, P.; Che, M.; Louis, C. *J. Phys. Chem. B* **1999**, *103*, 6171.
(20) Burattin, P.; Che, M.; Louis, C. *J. Phys Chem. B* **2000**, *104*, 10482.
(21) Higgins, J. B.; La Pierre, R. B.; Schlenker, J. L.; Rohrman, A. C.; Wood, J. D.; Kerr, G. T.; Rohrbaugh, W. J. *Zeolites* **1988**, *8*, 446.
(22) Treacy, M. M. J.; Newsam, J. M. *Nature* **1988**, *332*, 249.
(23) Camblor, M. A.; Corma, A.; Martínez, A.; Martínez-Soria, V.; Valencia, S. *J. Catal.* **1998**, *179*, 537.
(24) Jansen, J. C.; Creyghton, J.; Njo, S. L.; van Koningsveld, H.; van Bekkum, H. *Catal. Today* **1997**, *38*, 205.
(25) Babörek, E.; Nováková, J. *Appl. Catal.* **1999**, *185*, 123.
(26) Bécue, T.; Maldonado-Hodar, F. J.; Antunes, A. P.; Silva, J. M.; Ribeiro, M. F. *J. Catal.* **1999**, *181*, 244.
(27) Antunes, A. P.; Silva, J. M. Ribeiro, M. F. *J. Catal.* **1999**, *181*, 244.
(28) Mikkelsen, Ø.; Kolboe, S. *Micropor. Mater.* **1999**, *29*, 173.
(29) Halgeri, A. B.; Das, J. *Appl. Catal.* **1999**, *181*, 347.
(30) Nivarthy, G. S.; Seshan, K.; Lercher, J. A. *Micropor. Mater.* **1988**, *22*, 379.
(31) Zhang, W.; Smirniotis, P. G. *J. Catal.* **1999**, *182*, 400.
(32) Hermans, L. A.; Geus, J. W. In *Preparation of Catalysts II*; Delmon, B., Grange, P., Jacobs, P., Poncelet, G., Eds.; Elsevier: Amsterdam, 1997; p 113.
(33) Geus, J. W.; van Dillen, A. J. In *Preparation of Solid Catalysts*; Ertl, G., Knözinger, H., Weitkamp, J., Eds.; Wiley-VCH: Weinheim, 1999; p 460.
(34) Gregg, S. J.; Sing, K. S. W. *Adsorption, Surface Area and Porosity*; Academic Press: London and New York, 1967; p 173.
(35) Thomas, J. M.; Thomas, W. J. *Principles and Practice of Heterogeneous Catalysis*; Wiley-VCH: Weinheim, 1997; pp 257−318.
(36) Leofanti, G.; Padovan, M.; Tozzola, G.; Venturelli, V. *Catal. Today* **1998**, *41*, 207.
(37) Kiricsi, I.; Flego, C.; Pazzuconi, G.; Parker, W. O., Jr.; Millini, R.; Perego, C.; Bellussi, G. *J. Phys. Chem. B* **1994**, *98*, 4627.
(38) Bourgeat-Lami, E.; Massiani, P.; Di Renzo, F.; Espiau, P.; Fajula, F.; Des Courières T. *Appl. Catal.* **1991**, *72*, 139.
(39) Woolery, G. L.; Alemany, L. B.; Dessau, R. M.; Chester, A. W. *Zeolites* **1986**, *6*,14.
(40) Huger, M.; Kärger, J.; Pfeifer, H.; Caro, J.; Zibrowius, B.; Bülow, M. *J. Chem. Soc., Faraday Trans.* **1987**, *83*, 3429.
(41) Pérez-Pariente, J.; Sanz, J.; Fornés, V.; Corma, A. *Appl. Catal.* **1990**, *124*, 217.
(42) Trombetta, M.; Busca, G.; Storaro, L.; Lenarda, S.; Casagrande, M.; Zambon, A. *Phys. Chem. Chem. Phys.* **2000**, *2*, 3529.
(43) Szostak, R. *Molecular Sieves Principles of Synthesis and Identification*; Van Nostrand Reihold: New York, 1989; pp 282−347.
(44) Flanigen, E. M.; Word, J. W. In *Zeolite Chemistry and Catalysis ACS Monograph 171*; Rabo, J. A., Ed.; ACS Monograph 171 American Chemical Society: Washington, DC, 1976; pp 80−284.
(45) Breck, D. W. *Zeolite Molecular Sieve: Structure, Chemistry, and Use*; John Wiley & Son: New York, 1974; p 415.
(46) Coenen, J. W. E. *Appl. Catal.* **1989**, *54*, 65.
(47) Coenen, J. W. E. *Appl. Catal.* **1991**, 75, 193.